Schizophrenia Research 208 (2019) 308–316

Contents lists available at ScienceDirect

Schizophrenia Research

journal homepage: www.elsevier.com/locate/schres

Altered dynamic global signal topography in antipsychotic-naive adolescents with early-onset schizophrenia

Xiao Wang [a,b], Wei Liao [a,b], Shaoqiang Han [a,b], Jiao Li [a,b], Yan Zhang [c], Jingping Zhao [d,**], Huafu Chen [a,b,*]

[a] The Clinical Hospital of Chengdu Brain Science Institute, MOE Key Laboratory for Neuroinformation, University of Electronic Science and Technology of China, Chengdu 610054, China
[b] School of Life Science and Technology, Center for Information in BioMedicine, University of Electronic Science and Technology of China, Chengdu 610054, China
[c] Mental Health Institute, the Second Xiangya Hospital of Central South University, Key Laboratory for Mental Health of Hunan Province, Changsha, China
[d] Mental Health Institute, the Second Xiangya Hospital of Central South University, 139, Middle Renmin Road, Changsha, Hunan 410011, China

ARTICLE INFO

Article history:
Received 25 June 2018
Received in revised form 14 January 2019
Accepted 26 January 2019
Available online 14 February 2019

Keywords:
fMRI
early-onset schizophrenia
dynamic functional connectivity
BOLD
topography

ABSTRACT

Schizophrenia (SCZ) is a severe neuropsychiatric disease associated with dysfunction of brain regions and networks. Recent, functional magnetic resonance imaging (fMRI) studies have determined that the global signal (GS) is an important source of the local neuronal activity. However, the dynamics of this effect in SCZ remains unknown. To address this issue, 39 drug-naive patients with early-onset schizophrenia (EOS) and 31 age-, gender- and education-matched healthy controls underwent resting-state fMRI scans. Dynamic functional connectivity (DFC) was employed to assess the dynamic patterns of the GS in EOS. Dynamic analysis demonstrated that the topography of the GS in EOS can be divided into five different states. In the state1, the GS mainly affected the sensory regions. In the state2, the GS mainly affected the default mode network (DMN). In the state3, the GS mainly affected the frontoparietal network and the cingulate-opercular network. In the state4, the GS mainly affected the sensory and subcortical regions. In the state5, the GS mainly affected the sensory regions and DMN. In particular, the changes in the cerebellum, putamen and supramarginal gyrus was inversely proportional to the clinical symptoms. Our findings demonstrate that the influence of the GS on brain networks is dynamic and changes of this relationship may associate with clinical behavior in SCZ.

1. Introduction

Schizophrenia (SCZ) is a devastating and chronically debilitating brain disorder characterized by abnormal activity in local regions and networks (Heuvel and Fornito, 2014; Lancaster and Hall, 2016; Liao et al., 2018a; Mp et al., 2013). However, these abnormalities are often affected by multiple factors including environment, age and drugs in the pathological process (Erp et al., 2018; Liao et al., 2018a). Early-onset schizophrenia (EOS) provides an exceptional opportunity to explore the neuropathology of schizophrenia free from the potential confounds of prolonged periods of medication and disease interactions with age-related neurodegeneration (Epstein et al., 2014; Tonya et al., 2008; Wang et al., 2017; Zheng et al., 2017). Many studies have focused on exploration of the blood oxygen level-dependent (BOLD) signals in SCZ patients via functional magnetic resonance imaging (fMRI).

fMRI studies have captured differences in the BOLD signals between SCZ patients and healthy controls (HCs) in both task and resting states (Lowe, 2012). For example, by analyzing the variability of the BOLD signal in SCZ, Yang et al. found that the BOLD signal fluctuations in gray matter are more temporally variable in comparison with HCs, especially in the association regions (Yang et al., 2014b). Spatially specific changes in cortical BOLD patterns may represent a disruption in basic brain functions in SCZ and suggest that altered BOLD variability may impact functional connectivity estimates (Yang et al., 2014b). However, this conjecture is complicated by the use of global signal (GS) regression for resting-state fMRI (rs-fMRI) data (Fox et al., 2009b).

The GS is defined as the spatial average of time-varying BOLD signals across the brain. This signal is believed to reflect non-neuronal noise in many fMRI studies (Power et al., 2014; Power et al., 2016). Recently, however, controversy in the application of the GS to rs-fMRI analyses has been raised (Fox et al., 2009a; Murphy and Fox, 2016; Yang et al., 2016; Yang et al., 2014a) because the GS has also been showed to reflect important neurobiological information. For example, Wong et al. found that caffeine can lead to reductions in global amplitude and that this changed global signal amplitude is related to electroencephalographic vigilance in HCs (Chi et al., 2016; Wong et al., 2013). Yang et al. also found that the variability of the GS in patients with schizophrenia are

* Correspondence to: H. Chen, Key Laboratory for NeuroInformation of Ministry of Education, School of Life Science and Technology, University of Electronic Science and Technology of China, Chengdu 610054, China.
** Corresponding author.
E-mail addresses: zhaojingpingcsu@163.com (J. Zhao), chenhf@uestc.edu.cn (H. Chen).

https://doi.org/10.1016/j.schres.2019.01.035
0920-9964/

Table 1
Demographic and clinical characteristics.

Demographics, mean (SD)	EOS $N = 35$	Control $N = 30$	P value
Age (year)	15.5 (1.8)	15.3 (1.6)	0.57[a]
Gender (male/female)	20/15	13/17	0.27[b]
Education (years)	8.5 (1.48)	8.7 (1.42)	0.605[a]
Duration of psychosis (months)	16.0 (14.4)	–	–
Handedness (right/left)	35/0	30/0	–
PANSS positive symptoms	20.42 (5.72)	–	–
PANSS negative symptoms	20.91 (8.41)	–	–
PANSS general symptoms	33.28 (6.69)	–	–
PANSS total symptoms	74.62 (10.61)	–	–

P^a-value was obtained by two-sample t-test.
P^b-value was obtained by χ^2 two-tailed test.

related to schizophrenia symptoms (Yang et al., 2017; Yang et al., 2014b). Similar results have been obtained in studies on the autism spectrum (Gotts et al., 2012) and major depressive disorder (Zhu et al., 2018). These studies suggest that the GS is not merely nonneuronal physiological noise but also an important source of the neuronal activity itself, thus may contain important clinical information on psychiatric disorders. Moreover, the spatial topography of the GS, the representation of the GS in specific regions, has also been examined (Wen and Liu, 2016; Yang et al., 2016) and proposed a hypothesis that the clinical behavior are affected by this Spatiotemporal Psychopathology (Zhang et al., 2018). However, studies about the dynamic characteristics of this hypothesis is still lacking. Using a dynamic method to explore the spatiotemporal properties of the GS in EOS may provide a new way to understand the psychopathology in SCZ.

The current study aimed to assess the dynamic topography of the GS in EOS. The dynamic functional connectivity (DFC) method was employed to investigate the dynamic properties of the GS topography and two-sample t-tests were used for statistical analyses. The relationship between the aberrance and clinical symptoms was then investigated to test the contributions of pattern-specific alterations in coordination to the clinicopathology of EOS.

2. Materials and methods

2.1. Participants

A total of 39 patients with EOS and 31 age-, gender-, education-, and IQ-matched healthy adolescents were enrolled from the Second Affiliated Hospital of Xinxiang Medical University. All participants aged between 12 and 18 years, right-handed Han Chinese and had received >6 years of formal education. Exclusion criteria for all participants consisted of: (1) any past or current neurological disorders or family history of hereditary neurological disorders; (2) history of head injury with loss of consciousness; (3) alcohol or substance abuse; (4) claustrophobia; (5) MRI contraindications. Patients had to fulfill the following inclusion criteria: (1) diagnosis of schizophrenia according to DSM criteria (DSM-VI-TR); (2) no co-morbid Axis I diagnosis; (3) duration of illness <2 years; (4) no current or previous antipsychotic medication. Clinical symptoms were independently assessed by 2 experienced psychiatrists using DSM-VI based structured interviews (SCID-I/Patient version). To validate the initial diagnosis, all patients were re-assessed 6 months after the initial diagnostic interview (Li et al., 2018b; Wang et al., 2017). Clinical symptomatology was further evaluated using the Positive and Negative Syndrome Scale (PANSS).

This study was approved by the Ethics Committee of the Second Affiliated Hospital of Xinxiang Medical University, and informed written consents were obtained from all subjects.

2.2. Data acquisition

All subjects were instructed to rest with their eyes closed, not to think of anything in particular, and not to fall asleep during the rs-fMRI scan. fMRI data were acquired using the 3 T MRI scanner (Siemens-Trio, Erlangen, Germany) in the Second Affiliated Hospital of Xinxiang Medical University. Scanning and clinical assessments were performed in one day. Functional images were collected transversely using an echo-planar imaging (EPI) sequence with the following

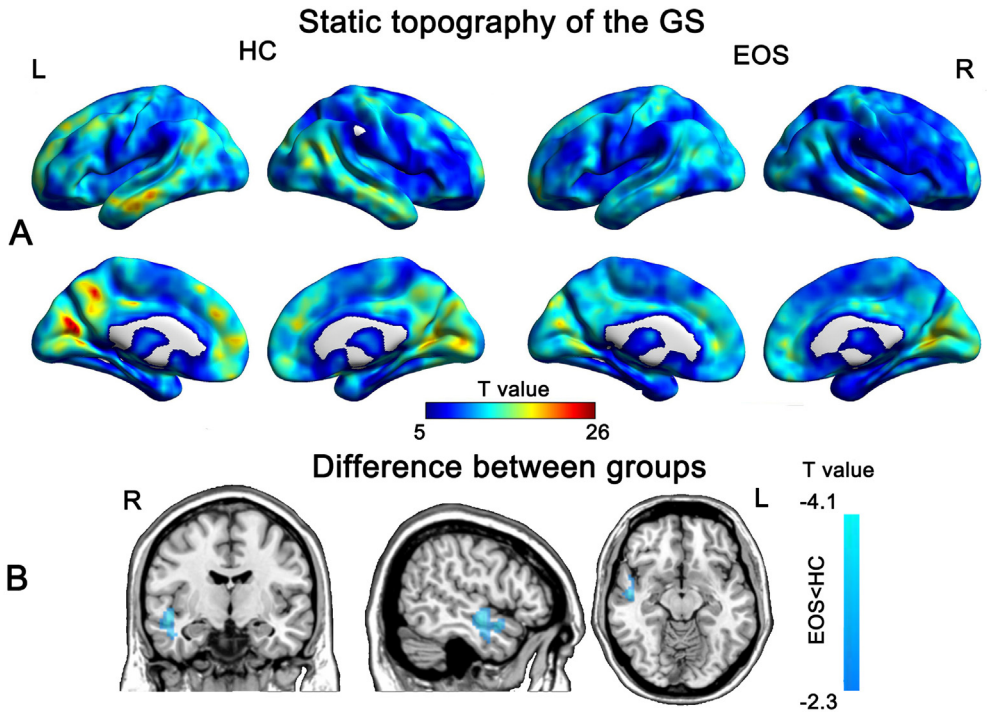

Fig. 1. Static topography of the GS and difference between the EOS and HC groups. (A) Surface visualization of group-level T-map computed across groups, left is the HC group, right is the EOS group. The T-map highlights positive FC values and covers virtually the entire brain. (B) GS representation is spatially altered in EOS. Cool color represents lower FC in the EOS than HC. GS, global signal; EOS, early-onset schizophrenia; HC, healthy control; FC, functional connectivity.

Table 2
Altered static topography of the GS in EOS compared with HC group.

Brain areas		L/R	Cluster size	T-value	Peak coordinate		
			voxels		X	Y	Z
EOS < HC	Superior temporal gyrus	R	112	−4.09	51	−9	−12

Statistical significance level is corrected for multiple comparisons using GRF theory with voxel significant $p < 0.01$, cluster significant $p < 0.05$. The peak coordinate is defined in MNI space. L, left. R, right.

settings: TR/TE = 2000/30 ms, flip angle = 90°, FOV = 220 × 220 mm^2, slices = 33, matrix = 64 × 64, interslice gap = 0.6 mm, and voxel size = 3.44 × 3.44 × 4 mm^3. The scan lasted for 480 s for each subject, and 240 volumes were acquired.

2.3. Image pre-processing

Data pre-processing was conducted using Statistical Parametric Mapping software (SPM8, http://www.fil.ion.ucl.ac.uk/spm8) following the steps of previous studies (Damaraju et al., 2014a; Fox et al., 2009b): (1) slice-time correction, (2) first 10 images removed from each run and (3) rigid-body motion correction. Four patients and one HC with head motion scans exceeding 2 mm or 1° rotation were excluded. The corrected images were subsequently normalised according to the standard SPM8 Montreal Neurological Institute (MNI) template and resampled to 3 × 3 × 3 mm^3 voxel size. Given that the resting-state GS is sensitive to minor head movements, all BOLD images were required to pass stringent quality assurance criteria: (i) signal-to-noise ratios (SNRs >100), which were computed following previous study (Fox et al., 2009b) and (ii) movement scrubbing. Here, we calculated the mean frame-wise displacement (FD) to determine the comparability of head movements across groups further. The largest mean FD of each subject was <0.3 mm and two-sample *t*-test showed that there was no significant difference in the mean FD between the two groups (HC: 0.09 ± 0.05; EOS: 0.10 ± 0.03. mean ± SD, $p = 0.33$). "Bad" time points (FD > 0.5 mm) as well as their 1-back and 2-forward time points were then scrubbed and interpolated by spline interpolation (Braun et al., 2016; Power et al., 2012). The resulting images were detrended and filtered. Finally, Friston 24 motion parameters, cerebrospinal fluid, and white matter signals were included in the multiple regression model to reduce the effects of head motion and non-neuronal BOLD fluctuations (Friston et al., 1994; Liao et al., 2018c).

2.4. Analysis of the static topography of the GS

We measured the static topography of the GS by using pairwise correlation between the GS time course and each voxel time course. The GS

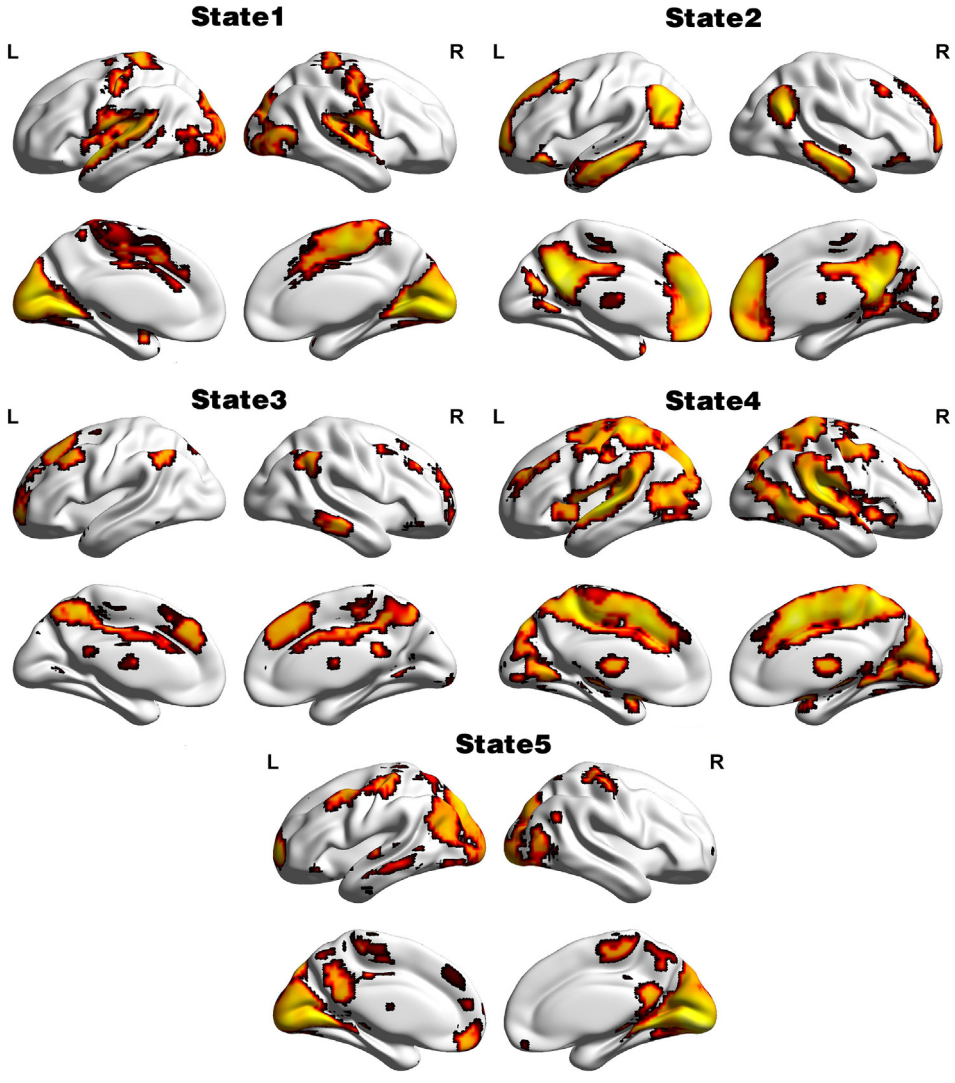

Fig. 2. Dynamic topography of the GS. DFC maps were clustered into five states. GS, global signal; DFC, dynamic functional connectivity.

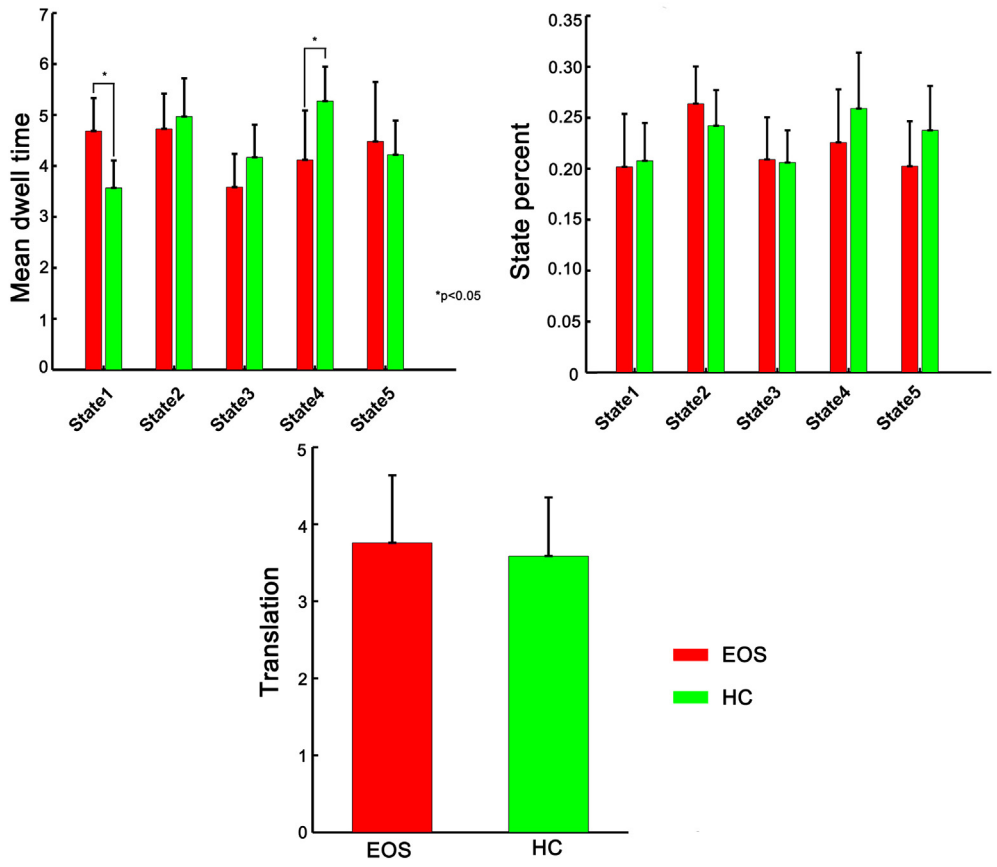

Fig. 3. Temporal properties of the GS topography in the EOS and HC groups. The red color and green color represent the EOS and HC groups, respectively.

time series for each subject was obtained by calculating the mean preprocessed BOLD signal averaged over all gray matter voxels for each time point, explicitly excluding ventricles and white matter signals. The correlation coefficients were then converted into z-values using Fisher's r-to-z transformation. In this work, the correlation map was computed by the FC method and the result was referred to as the stationary or static topography of the GS.

2.5. Analysis of the dynamic topography of the GS

To identify the dynamic patterns of the GS, we used a sliding window-based analytical method in the DynamicBC toolbox (Liao et al., 2018b; Liao et al., 2014; Liu et al., 2017). In sliding windows analysis, window length is an open area of research and an important parameter. In this work, we used the "rule of thumb", the minimum window length should be no less than $1/f_{min}$ (f_{min} was the minimum frequency of the correlating time courses) (Li et al., 2018a; Liao et al., 2018b), because short time segments would introduce spurious fluctuations (Leonardi and Van, 2015; Li et al., 2018c). We chose 50 TRs (100 s) as the sliding window length and shifted with a step size of 10 TRs (20s) followed the prior study (Li et al., 2018c). We also tried other parameters (widow width = 30TRs/40TRs, step = 10TRs and widow width = 50TRs, step = 2TRs/5TRs) to further examine the possible effects on the results. Then, we obtained 19 windows for each participant in total. In each sliding window, we computed the temporal correlation coefficient between the GS signal and each cortical voxel in the gray mask. Consequently, a set of sliding window correlation maps were created for each subject. Fisher's Z transformation was applied to all of the correlation maps to improve the normality of the correlation distribution (Yong et al., 2008; Zalesky et al., 2015).

2.6. Clustering

Based on our observation that patterns of global signal reoccur across windows and subjects, we used a k-means method to cluster the dynamic correlation maps, partitioning the data into a set of separate clusters to maximize the correlation within a cluster to the cluster centroid (Damaraju et al., 2014a). The optimal number of centroid states was estimated using the elbow criterion (Allen et al., 2014). A k of 5 was obtained using this method in a search cluster of k from 2 to

Table 3
Alterations of the GS topography in EOS at different states.

State		Brain areas	L/R	Cluster size	T-value	Peak coordinate		
				voxels		X	Y	Z
State1	EOS < HC	Middle temporal gyrus	R	85	−4.15	54	−66	6
State2	EOS < HC	Middle temporal gyrus	L	70	−3.67	−60	−18	−12
		Precuneus	L	80	−3.41	−3	−51	45
State3	EOS > HC	Cerebellum crus1	L	58	4.15	−33	−72	−24
		Middle cingulate gyrus	L	45	2.77	0	−6	33
State4	EOS > HC	Putamen	R	51	2.80	36	−15	−6
		Precuneus	R	70	3.14	−15	−51	66
		Supramarginal gyrus	R	61	2.76	57	−36	39
State5	EOS < HC	Calcarine	L	124	−3.33	0	−87	0

Statistical significance level is corrected for multiple comparisons using GRF theory with voxel significant $p < 0.01$, cluster significant $p < 0.05$. The peak coordinate is defined in MNI space. L, left. R, right.

9. The correlation coefficient was chosen as it is more sensitive to the connectivity pattern regardless of magnitude (Damaraju et al., 2014a; Li et al., 2018d). We also tried other parameters (widow width = 30TRs/40TRs, step =10TRs and widow width = 50TRs, step = 2TRs/5TRs) to further examine the possible effects on clustering (Fig. S3).

2.7. Dynamic topological metrics

To examine the temporal properties of DFC states, we assessed three commonly summary metrics including mean dwell time, fractional windows and number of transitions. The mean dwell time represents how long the participant stayed in a certain state, which was calculated by averaging the number of consecutive windows belonging to one state before changing to the other state. The fractional window is the proportion of time spent in each state as measured by percentage. The number of transitions represents how many times either state changed from one to the other, counting the number of times a switch occurred, with more transitions representing less stability over time (Kim et al., 2017). The significance of these metrics between the HC and EOS groups was tested using two-sample *t*-tests.

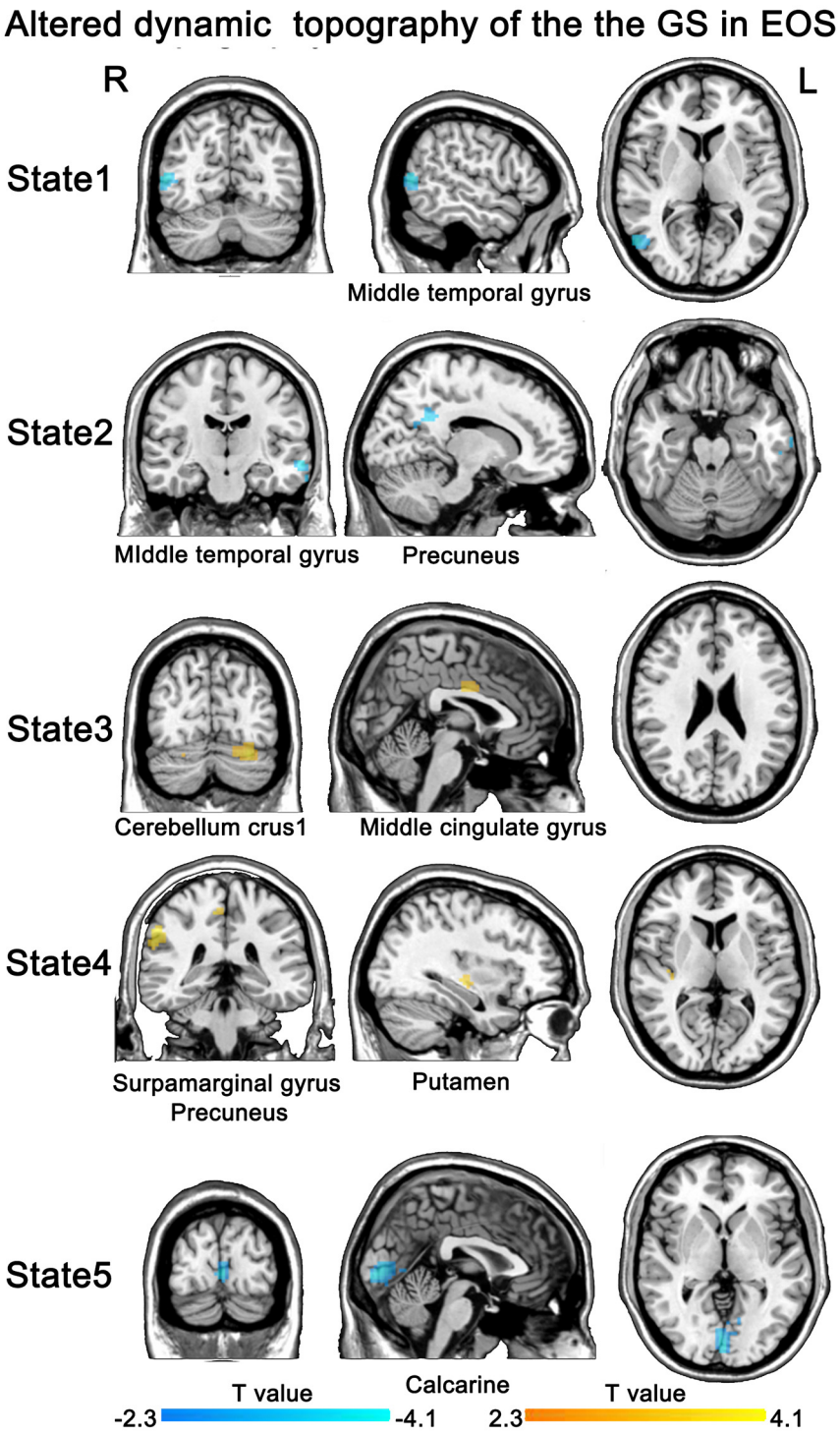

Fig. 4. Altered dynamic topography of the GS in EOS group compared with HC group. Cool color represents lower FC in the EOS than HC. GS, global signal; FC, functional connectivity; EOS, early-onset schizophrenia; HC, healthy control.

2.8. Statistical analysis

For each state, one-sample *t*-test was performed for each group. The significance level was set to $p < 0.05$ (Gaussian random field (GRF) corrected) (Wenbin et al., 2015). Differences in the static topography of the GS between the EOS and HC groups were measured using the two-sample *t*-test analysis. To examine the differences in spatiotemporal properties of the GS between the two groups, two-sample *t*-test analysis was employed. Given that age and gender may affect the results in SCZ, they were considered as covariates in the above analyses (Maccabe et al., 2004). GRF theory was used for correction of cluster-level multiple comparisons (voxel significance $p < 0.01$, cluster significance $p < 0.05$). Brain regions showing significant differences based on the results of two-sample *t*-test during the dynamic analysis were defined as regions of interests (ROIs) for the following analysis. ROIs were defined as a 6 mm spheres with a centre at the peak position of statistical difference. Correlation analysis was then performed between the mean FC in the ROIs and the PANSS scores of the EOS patients.

3. Results

3.1. Demographics and clinical symptoms

There were no significant differences were found in gender, age, and years of education between the EOS and HC groups. For the patient group, the mean duration of illness was 16.0 months (SD = 14.4) (Table 1).

3.2. Static topography of the GS

The static topography of the GS is showed in Fig. 1. The static topography of the GS in the EOS and HC groups showed a non-uniform distribution. The static topography of the GS was significantly lower in the EOS group compared with the healthy control group. Reduced FC was mainly found in the right superior temporal gyrus (Table 2) (GRF correction: voxel significant $p < 0.01$, cluster significant $p < 0.05$).

3.3. Dynamic topography of the GS

The dynamic spatial patterns of the GS are showed in Fig. 2. DFC maps were classified into five spatial patterns. State1 mainly included the temporal lobe, occipital lobe and inferior parietal lobule. State2 mainly included the posterior cingulate gyrus, anterior cingulate gyrus, middle temporal gyrus, frontal lobe, thalamus, angular. State3 mainly included the temporal pole, subcortical, middle frontal gyrus, cingulate gyrus, supramarginal gyrus, cerebellum and inferior parietal gyrus. State4 mainly included the temporal lobe, parietal-motor regions, occipital lobe, middle frontal gyrus and subcortical regions. State5 mainly included the temporal pole, occipital lobe, superior frontal gyrus medial orbital, thalamus, posterior cingulate gyrus and

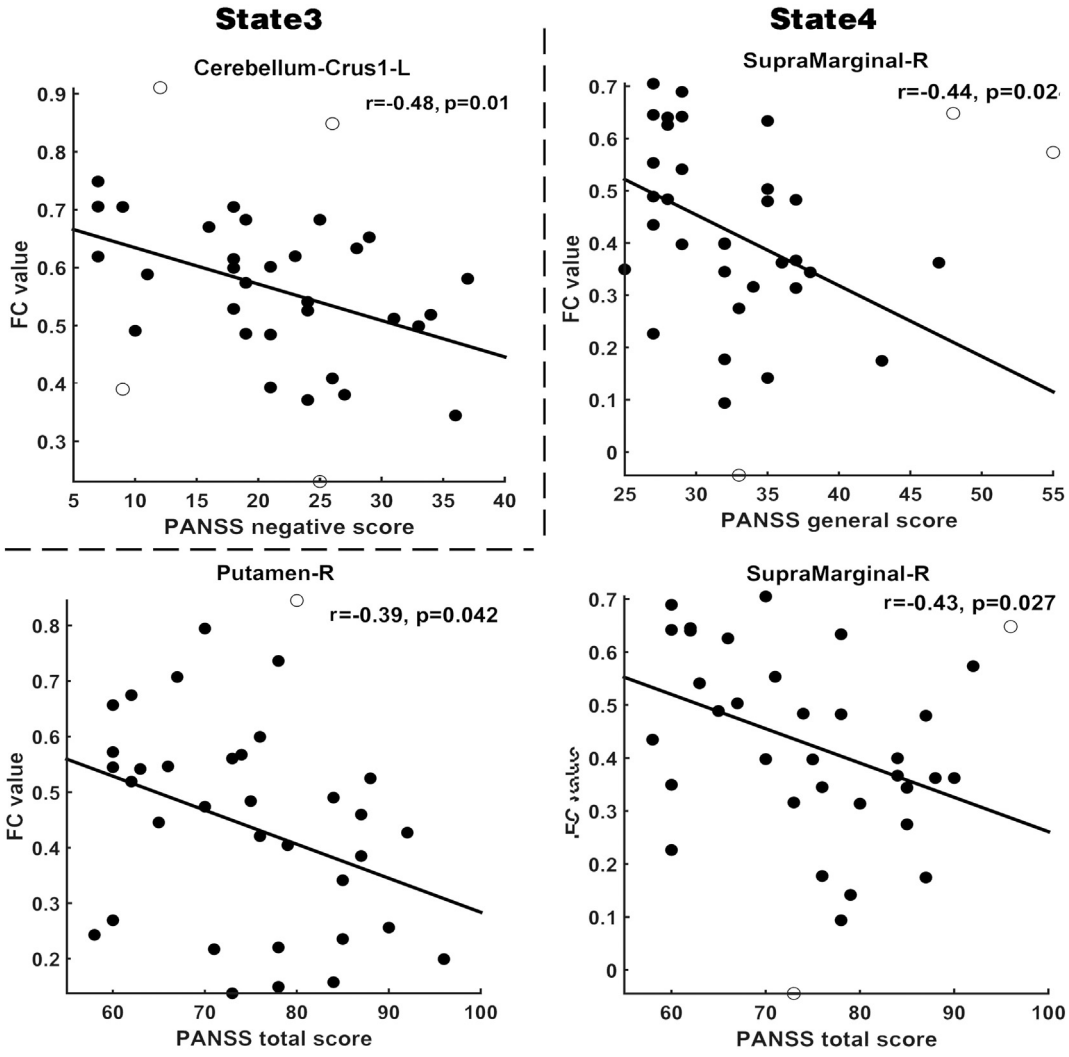

Fig. 5. Correlation between regions showed altered synchronism and clinical scale of symptoms in patients with EOS ($p < 0.05$, uncorrected). Shepherd's *pi* correlations were calculated over the data after removing outliers.

precentral gyrus. Specially, we found the state5 was most similar to the static GS topography (The correlation between all states and the static: state1: $r = 0.51$; state2: $r = 0.68$; state3: $r = 0.64$; state4: $r = 0.55$; state5: $r = 0.75$).

3.4. Temporal properties of the GS topography

As showed in the Fig. 3, significant group differences were identified in the mean dwell time in state1 and state4. Specifically, the mean dwell time in the state1 was significantly longer in the EOS group compared with the healthy control group (mean ± SD windows, for HC: 3.57± 1.06; for EOS patients: 4.68 ± 1.21, $p < 0.05$, uncorrected). In contrast, the mean dwell time in the state4 was significantly shorter in the EOS group compared to the healthy control group (mean ± SD windows, for HC: 5.27 ± 1.31; for EOS patients: 4.11 ± 1.63, $p < 0.05$, uncorrected).

3.5. Alterations of the GS topography in EOS at different states

Prior work shows that the GS and spatial pattern of the GS representation are altered in SCZ relative to HCs (Yang et al., 2017; Yang et al., 2014b). We thus hypothesised that the spatial pattern of the GS in EOS is also altered and the changing is dynamic. To test the hypotheses, we computed a T-map comparing the EOS group with the HC group at different patterns (Table 3). The results revealed that in state1, patients with EOS showed decreased FC in the right middle temporal gyrus (GRF: voxel significant $p < 0.01$, cluster significant $p < 0.05$). In state2, patients with EOS showed reduced FC in the left middle temporal gyrus and left precuneus (GRF correction: voxel significant $p < 0.01$, cluster significant $p < 0.05$). In state3 patients with EOS showed increased FC in the left cerebellum crus 1 and left middle cingulate gyrus (GRF correction: voxel significant $p < 0.01$, cluster significant $p < 0.05$). In state4, patients with EOS showed increased FC in the right putamen, right precuneus, and right supramarginal gyrus (GRF correction: voxel significant $p < 0.01$, cluster significant $p < 0.05$). Finally, in state5, patients with EOS showed reduced FC in the left calcarine (GRF correction: voxel significant $p < 0.01$, cluster significant $p < 0.05$) (see Fig. 4).

3.6. Correlation with clinical symptoms

Shepherd's *pi* correlation, defined by Rousselet and Pernet, was calculated between the FC of the ROIs in the different states and PANSS scores after removal of potential outliers (Rousselet and Pernet, 2012; Schwarzkopf et al., 2012). In the Fig. 5 the left cerebellum crus1 with reduced FC is significantly negatively correlated with the negative PANSS scores in state 3. In state4, the right supramarginal gyrus with reduced FC is significantly negatively correlated with the general and total scores of PANSS, and the right putamen with reduced FC shows a significantly negatively correlation with the total scores of PANSS.

4. Discussion

In this study, we used the DFC method to investigate the dynamic changes in the GS topography in EOS patients. We identified five different topography patterns of the GS. Patients with EOS showed state-specific differences compared with the HC group. Differences in the left cerebellum crus1, right putamen and supramarginal gyrus were significantly correlated with the clinical symptoms in state3 and state4. Our findings shed lights on the neuronal mechanisms of psychopathological symptoms in EOS, and its relevance in the dynamic relationship between global and networks activities for behavior in general.

4.1. Static topography of the GS in EOS

Different and non-uniform distributions of the GS topography were found in the HC and EOS groups. In the right superior temporal gyrus, EOS patients showed significantly lower FC compared with the HC. We also used the Power's template to divide the association regions and sensory regions for comparison, but no positive result was found (S4). These inconsistent results may be due to the sample selection. Previous research had found inconsistent results between adult-onset (Yong et al., 2008) and early-onset (Alexander-Bloch et al., 2010) schizophrenia in the global topological properties. The current findings supported the hypothesis that the GS topography abnormalities exist in SCZ patients, and suggest that the abnormalities of the GS topography may related with the different SCZ samples.

4.2. Altered dynamic topography of the GS in EOS

The dynamic patterns of the GS were divided into five different states by clustering all of the topography maps across windows and subjects. State1 mainly includes the visual cortex, the auditory cortex and the somatosensory cortex. State2 mainly includes the default mode network (DMN). State3 mainly includes the frontoparietal network and cingulate-opercular network. State4 mainly includes the somatosensory cortex, the visual cortex, the auditory cortex and subcortical regions. State5 mainly includes the posterior-DMN, the somatosensory cortex and the visual cortex.

4.2.1. Altered temporal properties of the dynamic topography

Then, we made statistics on the temporal properties of the five states. Results revealed that EOS patients showed longer mean dwell time in the state1 and shorter mean dwell time in the state4 compared with HC. According to the spatial distribution (Admon et al., 2015; Fornito et al., 2013) of the different states, we found that the state1 mainly includes the sensory regions and the state4 mainly includes the sensory and subcortical network. Sensory network, as an important functional network, senses and integrates information from inside and outside the brain (Javitt, 2009). The subcortical regions are involved in information processing and regulation (Johnstone et al., 2007). The dysfunction of them is thought to be associated with the positive symptoms in SCZ patients (Keshavan et al., 2014). Our results provide a new possible mechanism for the abnormal activity of sensory and subcortical regions in SCZ.

4.2.2. State-specific differences between the EOS and HC groups

State-specific differences between the EOS and HC groups were further detected. In state1 patients with EOS showed reduced FC in the right middle temporal gyrus. Middle temporal gyrus plays an integrative role in visual and auditory information, and its structural and functional abnormalities are commonly reported in SCZ (Hu et al., 2013), and the dysfunction of it was thought to be associated with the positive symptoms in SCZ, such as hallucination (Cui et al., 2017). In the state2, patients showed decreased FC in the left middle temporal gyrus and left precuneus. The precuneus, as important region of DMN, is considered the center of a wide spectrum of highly integrated tasks (Utevsky et al., 2014). In the state3, patients with EOS showed increased FC in the left cerebellum crus1 and left middle cingulate gyrus. Cerebellum crus1 is involved in processing, especially in the sensorimotor control, is related to schizophrenia (Wang et al., 2017). In the state4, patients showed increased FC in the right putamen, right precuneus and right supramarginal gyrus.

Our findings are in line with the results of previous studies (Damaraju et al., 2014b; Murray and Anticevic, 2016; Rashid et al., 2016), that is, schizophrenia is associated with abnormalities in the dopamine and the sensory systems. Moreover, in the state5, patients with EOS showed decreased FC in the left calcarine. Calcarine is an important part of the primary visual cortex involving the visual processing (Celesia et al., 1980). Our results provide a new possible neural mechanism to explain the functional abnormalities of different brain regions and networks in SCZ.

4.3. Correlation analysis

In state3, the changes in the FC in the left cerebellum crus1 correlated with the scores of PANSS. In the state4, changes in the FC in the putamen and supramarginal gyrus correlated with the scores of PANSS. The current findings suggest the clinical symptoms are consequently dominated by sensorimotor and dopamine system regions and the psychopathological symptoms could be traced to an abnormal spatial structure in the topographical distribution of the GS. Our results provided new supplement for the hypothesis that the abnormalities in SCZ is affected in Spatiotemporal Psychopathology.

5. Limitation

The limitations of the current study should be considered. The size of our sample was relatively small. However, given that the incidence of the EOS, it is comparable. A larger size of sample is needed to confirm the results in the current study. In the data collection design, we did not consider the physiological noise (cardiovascular and respiratory), which may lead to some inconsistent results compared with the previous study. In the following research, we will refine our experimental design.

6. Conclusion

In this study, we explored alterations in dynamic topography of the GS in EOS. Five different patterns were found. State-specific differences were also found mainly in the sensorimotor network, the subcortical network and the default mode network. A significant negative correlation between the altered FC and clinical symptoms at a specific state was found in the cerebellum, putamen, and supramarginal gyrus, thereby, implying that the clinical symptoms are related to the altered dynamic spatial structure in the topographical distribution of the GS. Our observations may provide potential implications for exploring in schizophrenia further.

Contributors

Yan Zhang designed the study and conceptualized the protocol for healthy subjects. Jingping Zhao and Huafu Chen adapted this protocol for schizophrenia patients and evaluated them. Wei Liao and Shaoqiang Han managed the literature searches and analyses. Xiao Wang and Jiao Li undertook the statistical analyses, and Xiao Wang wrote the first draft of the manuscript. All authors contributed to and have approved the final manuscript.

Acknowledgements

This research was supported by the Natural Science Foundation of China (61533006 and 61673089), the project of the Science and Technology Department of Sichuan Province (2017JY0094), the Fundamental Research Funds for Central Universities (ZYGX2016KYQD120 and ZYGX2015J141) and the Sichuan Science and Technology Program (2018TJPT0016).

Appendix A. Supplementary data

Supplementary data to this article can be found online at https://doi.org/10.1016/j.schres.2019.01.035.

References

Admon, R., Nickerson, L.D., Dillon, D.G., Holmes, A.J., Bogdan, R., Kumar, P., Dougherty, D.D., Iosifescu, D.V., Mischoulon, D., Fava, M., 2015. Dissociable cortico-striatal connectivity abnormalities in major depression in response to monetary gains and penalties. Psychol. Med. 45 (1), 121–131.

Alexander-Bloch, A.F., Gogtay, N., Meunier, D., Birn, R., Clasen, L., Lalonde, F., Lenroot, R., Giedd, J., Bullmore, E.T., 2010. Disrupted modularity and local connectivity of brain functional networks in childhood-onset schizophrenia. Front. Syst. Neurosci. 4, 147.

Allen, E.A., Eswar, D., Plis, S.M., Erhardt, E.B., Tom, E., Calhoun, V.D., 2014. Tracking whole-brain connectivity dynamics in the resting state. Cereb. Cortex 24 (3), 663–676.

Braun, U., Schäfer, A., Bassett, D.S., Rausch, F., Schweiger, J.I., Bilek, E., Erk, S., Romanczuk-Seiferth, N., Grimm, O., Geiger, L.S., 2016. Dynamic brain network reconfiguration as a potential schizophrenia genetic risk mechanism modulated by NMDA receptor function. Proc. Natl. Acad. Sci. U. S. A. 113 (44), 12568.

Celesia, G.G., Archer, C.R., Kuroiwa, Y., Goldfader, P.R., 1980. Visual function of the extrageniculo-calcarine system in man: relationship to cortical blindness. Arch. Neurol. 37 (11), 704.

Chi, W.W., Deyoung, P.N., Liu, T.T., 2016. Differences in the resting-state fMRI global signal amplitude between the eyes open and eyes closed states are related to changes in EEG vigilance. NeuroImage 124 (Pt A), 24.

Cui, Y., Liu, B., Song, M., Lipnicki, D.M., Li, J., Xie, S., Chen, Y., Li, P., Lu, L., Lv, L., 2017. Auditory verbal hallucinations are related to cortical thinning in the left middle temporal gyrus of patients with schizophrenia. Psychol. Med. 48 (1), 1–8.

Damaraju, E., Allen, E.A., Belger, A., Ford, J.M., Mcewen, S., Mathalon, D.H., Mueller, B.A., Pearlson, G.D., Potkin, S.G., Preda, A., 2014a. Dynamic functional connectivity analysis reveals transient states of dysconnectivity in schizophrenia. Neuroimage Clin. 5 (C), 298–308.

Damaraju, E., Allen, E.A., Belger, A., Ford, J.M., Mcewen, S., Mathalon, D.H., Mueller, B.A., Pearlson, G.D., Potkin, S.G., Preda, A., 2014b. Dynamic functional connectivity analysis reveals transient states of dysconnectivity in schizophrenia. Neuroimage Clin. 5 (C), 298–308.

Epstein, K.A., Cullen, K.R., Mueller, B.A., Robinson, P., Lee, S., Kumra, S., 2014. White matter abnormalities and cognitive impairment in early-onset schizophrenia-spectrum disorders. J. Am. Acad. Child Adolesc. Psychiatry 53 (3), 362–372.e362.

Erp, T.G.V., Walton, E., Hibar, D.P., Schmaal, L., Jiang, W., Glahn, D.C., Pearlson, G.D., Yao, N., Fukunaga, M., Hashimoto, R., 1 November 2018. Cortical brain abnormalities in 4474 individuals with schizophrenia and 5098 controls via the ENIGMA consortium. Biol. Psychiatry 84 (9), 644–654.

Fornito, A., Harrison, B.J., Goodby, E., Dean, A., Ooi, C., Nathan, P.J., Lennox, B.R., Jones, P.B., Suckling, J., Bullmore, E.T., 2013. Functional dysconnectivity of corticostriatal circuitry as a risk phenotype for psychosis. Jama Psychiatry 70 (11), 1143–1151.

Fox, M.D., Dongyang, Z., Snyder, A.Z., Raichle, M.E., 2009a. The global signal and observed anticorrelated resting state brain networks. J. Neurophysiol. 101 (6), 3270–3283.

Fox, M.D., Zhang, D., Snyder, A.Z., Raichle, M.E., 2009b. The global signal and observed anticorrelated resting state brain networks. J. Neurophysiol. 101 (6), 3270–3283.

Friston, K.J., Holmes, A.P., Worsley, K.J., Poline, J.P., Frith, C.D., Frackowiak, R.S.J., 1994. Statistical parametric maps in functional imaging: a general linear approach. Hum. Brain Mapp. 2 (4), 189–210.

Gotts, S.J., Simmons, W.K., Milbury, L.A., Wallace, G.L., Cox, R.W., Martin, A., 2012. Fractionation of social brain circuits in autism spectrum disorders. Brain J. Neurol. 135 (Pt 9), 2711–2725.

Heuvel, M.P.V.D., Fornito, A., 2014. Brain networks in schizophrenia. Neuropsychol. Rev. 24 (1), 32–48.

Hu, M., Li, J., Eyler, L., Guo, X., Wei, Q., Tang, J., Liu, F., He, Z., Li, L., Jin, H., 2013. Decreased left middle temporal gyrus volume in antipsychotic drug-naive, first-episode schizophrenia patients and their healthy unaffected siblings. Schizophr. Res. 144 (1–3), 37–42.

Javitt, D.C., 2009. Sensory processing in schizophrenia: neither simple nor intact. Schizophr. Bull. 35 (6), 1059.

Johnstone, T., van Reekum, C.M., Urry, H.L., Kalin, N.H., Davidson, R.J., 2007. Neurobiology of disease failure to regulate: counterproductive recruitment of top-down prefrontal-subcortical circuitry in major depression. J. Neurosci. 27 (33), 8877–8884.

Keshavan, M.S., Giedd, J., Lau, J.Y., Lewis, D.A., Paus, T., 2014. Changes in the adolescent brain and the pathophysiology of psychotic disorders. Lancet Psychiatry 1 (7), 549–558.

Kim, J., Criaud, M., Cho, S.S., Dã-Ez-Cirarda, M., Mihaescu, A., Coakeley, S., Ghadery, C., Valli, M., Jacobs, M.F., Houle, S., 2017. Abnormal intrinsic brain functional network dynamics in Parkinson's disease. Brain 140 (11).

Lancaster, T.M., Hall, J., 2016. Altered intra- and inter-network dynamics reflect symptom dimensions in childhood-onset schizophrenia. Brain J. Neurol. 139 (Pt 1), 10.

Leonardi, N., Van, D.V.D., 2015. On spurious and real fluctuations of dynamic functional connectivity during rest. NeuroImage 104, 464–465.

Li, J., Duan, X., Cui, Q., Chen, H., Liao, W., 2018a. More than just statics: temporal dynamics of intrinsic brain activity predicts the suicidal ideation in depressed patients. Psychol. Med. 1–9.

Li, M., Becker, B., Zheng, J., Zhang, Y., Chen, H., Liao, W., Duan, X., Liu, H., Zhao, J., Chen, H., 2018b. Dysregulated maturation of the functional connectome in antipsychotic-naïve, first-episode patients with adolescent-onset schizophrenia. Schizophr. Bull. https://doi.org/10.1093/schbul/sby063.

Li, R., Liao, W., Yu, Y., Chen, H., Guo, X., Tang, Y.L., Chen, H., 2018c. Differential patterns of dynamic functional connectivity variability of striato-cortical circuitry in children with benign epilepsy with centrotemporal spikes. Hum. Brain Mapp. 39 (3), 1207–1217.

Li, R., Liao, W., Yu, Y., Chen, H., Guo, X., Tang, Y.L., Chen, H., 2018d. Differential patterns of dynamic functional connectivity variability of striato–cortical circuitry in children with benign epilepsy with centrotemporal spikes. Hum. Brain Mapp. 39 (3), 1207–1217.

Liao, W., Wu, G.R., Xu, Q., Ji, G.J., Zhang, Z., Zang, Y.F., Lu, G., 2014. DynamicBC: a MATLAB toolbox for dynamic brain connectome analysis. Brain Connect. 4 (10), 780.

Liao, W., Fan, Y.-S., Yang, S., Li, J., Duan, X., Cui, Q., Chen, H., 2018a. Preservation effect: cigarette smoking acts on the dynamic of influences among unifying neuropsychiatric triple networks in schizophrenia. Schizophr. Bull. https://doi.org/10.1093/schbul/sby184.

Liao, W., Li, J., Duan, X., Cui, Q., Chen, H., Chen, H., 2018b. Static and dynamic connectomics differentiate between depressed patients with and without suicidal ideation. Hum. Brain Mapp. 39 (10), 4105–4118.

Liao, W., Yang, S., Li, J., Fan, Y.-S., Duan, X., Cui, Q., Chen, H., 2018c. Nicotine in action: cigarette smoking modulated homotopic functional connectivity in schizophrenia. Brain Imaging Behav. 1–12.

Liu, F., Wang, Y., Li, M., Wang, W., Li, R., Zhang, Z., Lu, G., Chen, H., 2017. Dynamic functional network connectivity in idiopathic generalized epilepsy with generalized tonic-clonic seizure. Hum. Brain Mapp. 38 (2), 957–973.

Lowe, M.J., 2012. The emergence of doing "nothing" as a viable paradigm design. NeuroImage 62 (2), 1146–1151.
Maccabe, J.H., Eranti, S.S., Sham, P.C., Everitt, B.S., Murray, R.M., 2004. Gender differences in age at onset in schizophrenia: a meta-analysis and meta-regression examining the effects of family history and study design. Schizophr. Res. 57–58.
Mp, V.D.H., Sporns, O., Collin, G., Scheewe, T., Mandl, R.C., Cahn, W., Goñi, J., Hulshoff Pol, H.E., Kahn, R.S., 2013. Abnormal rich club organization and functional brain dynamics in schizophrenia. Jama Psychiatry 70 (8), 783–792.
Murphy, K., Fox, M.D., 2016. Towards a consensus regarding global signal regression for resting state functional connectivity MRI. NeuroImage 154.
Murray, J.D., Anticevic, A., 2016. Toward understanding thalamocortical dysfunction in schizophrenia through computational models of neural circuit dynamics. Schizophr. Res. 180, 70–77.
Power, J.D., Barnes, K.A., Snyder, A.Z., Schlaggar, B.L., Petersen, S.E., 2012. Spurious but systematic correlations in functional connectivity MRI networks arise from subject motion. NeuroImage 63 (2), 999.
Power, J.D., Mitra, A., Laumann, T.O., Snyder, A.Z., Schlaggar, B.L., Petersen, S.E., 2014. Methods to detect, characterize, and remove motion artifact in resting state fMRI. NeuroImage 84 (1), 320–341.
Power, J.D., Plitt, M., Laumann, T.O., Martin, A., 2016. Sources and implications of whole-brain fMRI signals in humans. NeuroImage 146, 609–625.
Rashid, B., Arbabshirani, M.R., Damaraju, E., Cetin, M.S., Miller, R., Pearlson, G.D., Calhoun, V.D., 2016. Classification of schizophrenia and bipolar patients using static and dynamic resting-state fMRI brain connectivity. NeuroImage 134, 645–657.
Rousselet, G.A., Pernet, C.R., 2012. Improving standards in brain-behavior correlation analyses. Front. Hum. Neurosci. 6 (13), 119.
Schwarzkopf, D.S., Haas, B.D., Rees, G., 2012. Better ways to improve standards in brain-behavior correlation analysis. Front. Hum. Neurosci. 6 (6), 200.
Tonya, W., Kathryn, C., Lisa Michelle, R., Canan, K., Monica, L., Marcus, S., Donaya, H., Sanjiv, K., Schulz, S., Charles, Lim, 2008. Limbic structures and networks in children and adolescents with schizophrenia. Schizophr. Bull. 34 (1), 18.
Utevsky, A.V., Smith, D.V., Huettel, S.A., 2014. Precuneus is a functional core of the default-mode network. J. Neurosci. 34 (3), 932.
Wang, X., Zhang, Y., Long, Z., Zheng, J., Zhang, Y., Han, S., Wang, Y., Duan, X., Yang, M., Zhao, J., 2017. Frequency-specific alteration of functional connectivity density in antipsychotic-naive adolescents with early-onset schizophrenia. J. Psychiatr. Res. 95, 68.
Wen, H., Liu, Z., 2016. Broadband electrophysiological dynamics contribute to global resting-state fMRI signal. J. Neurosci. 36 (22), 6030–6040.
Wenbin, G., Feng, L., Changqing, X., Miaoyu, Y., Zhikun, Z., Jianrong, L., Jian, Z., Jingping, Z., 2015. Increased causal connectivity related to anatomical alterations as potential endophenotypes for schizophrenia. Medicine 94 (42), e1493.
Wong, C.W., Olafsson, V., Tal, O., Liu, T.T., 2013. The amplitude of the resting-state fMRI global signal is related to EEG vigilance measures. NeuroImage 83 (12), 983–990.
Yang, G.J., Murray, J.D., Grega, R., Cole, M.W., Aleksandar, S., Glasser, M.F., Christopher, P., Krystal, J.H., Xiao-Jing, W., Pearlson, G.D., 2014a. Altered global brain signal in schizophrenia. Proc. Natl. Acad. Sci. U. S. A. 111 (20), 7438–7443.
Yang, G.J., Murray, J.D., Repovs, G., Cole, M.W., Savic, A., Glasser, M.F., Pittenger, C., Krystal, J.H., Wang, X.J., Pearlson, G.D., 2014b. Altered global brain signal in schizophrenia. Proc. Natl. Acad. Sci. U. S. A. 111 (20), 7438–7443.
Yang, G.J., Murray, J.D., Glasser, M., Pearlson, G.D., Krystal, J.H., Schleifer, C., Repovs, G., Anticevic, A., 2016. Altered global signal topography in schizophrenia. Cereb. Cortex 27 (11).
Yang, G.J., Murray, J.D., Glasser, M., Pearlson, G.D., Krystal, J.H., Schleifer, C., Repovs, G., Anticevic, A., 1 November 2017. Altered global signal topography in schizophrenia. Cereb. Cortex 27 (11), 5156–5169.
Yong, L., Meng, L., Yuan, Z., Yong, H., Yihui, H., Ming, S., Chunshui, Y., Haihong, L., Zhening, L., Tianzi, J., 2008. Disrupted small-world networks in schizophrenia. Brain 131 (4), 945–961.
Zalesky, A., Pantelis, C., Cropley, V., Fornito, A., Cocchi, L., Mcadams, H., Clasen, L., Greenstein, D., Rapoport, J.L., Gogtay, N., 2015. Delayed development of brain connectivity in adolescents with schizophrenia and their unaffected siblings. Jama Psychiatry 72 (9), 900.
Zhang, J., Magioncalda, P., Huang, Z., Tan, Z., Hu, X., Hu, Z., Conio, B., Amore, M., Inglese, M., Martino, M., 2018. Altered global signal topography and its different regional localization in motor cortex and hippocampus in mania and depression. Schizophr. Bull. https://doi.org/10.1093/schbul/sby138.
Zheng, J., Zhang, Y., Li, M., Liao, W., Duan, X., Zhao, J., Chen, H., 2017. Aberrant corticostriatal connectivity predict positive symptoms of antipsychotic-naïve patients with adolescent-onset schizophrenia during brain maturation. Schizophr. Res. 195 S0920996417306539.
Zhu, J., Cai, H., Yuan, Y., Yue, Y., Jiang, D., Chen, C., Zhang, W., Zhuo, C., Yu, Y., 2018. Variance of the global signal as a pretreatment predictor of antidepressant treatment response in drug-naïve major depressive disorder. Brain Imaging Behav. 1–7.